Bull. Chem. Soc. Jpn., 72, 1717—1729 (1999)

Classification of Low-Energy Conformations of Met-Enkephalin in the Gas Phase and in a Model Solvent Based on the Extended Scaled Particle Theory

Ayori Mitsutake, Masayuki Irisa,† Yuko Okamoto,* and Fumio Hirata*

Department of Functional Molecular Science, The Graduate University for Advanced Studies, and Department of Theoretical Studies, Institute for Molecular Science, Okazaki, Aichi 444-8585

†Department of Biochemical Science and Engineering, Kyushu Institute of Technology, Iitsuka, Fukuoka 820-8502

(Received January 13, 1999)

We employed Monte Carlo simulated annealing to classify the low-energy conformations of Met-enkephalin in the gas phase and in aqueous solution. In order to include the free energy of cavity formation in aqueous solution, we used the method of extended scaled particle theory. This is the first attempt to combine the Monte Carlo simulated annealing method and the extended scaled particle theory. We conducted 20 Monte Carlo simulated annealing runs of 10000 Monte Carlo sweeps both in the gas phase and in aqueous solution. It was found that the obtained conformations (20 each) can be classified into 3 groups of similar structure both in the gas phase and in aqueous solution. We studied in detail the structural characteristics of the classified conformations. It was found that the cavity-formation effects of aqueous solution do not drastically change the backbone structures obtained in the gas phase. The relation between the solvent-accessible surface area and the cavity-formation free energy was studied in detail. The results show unambiguously that the cavity-formation free energy is not neccessarily proportional to the accessible surface area, at least for a small peptide.

It is widely believed that the folded conformation of a globular protein is determined solely by its amino-acid sequence information. The structure of a native protein corresponds to the conformation with the lowest free energy. Much effort has been invested to find such conformations for peptide and protein molecules. There are two difficulties in predicting the tertiary structure of a protein. One lies in the fact that there exist a huge number of local minima in the potential energy function, which makes it prohibitively difficult to apply standard sampling algorithms in search of the global minimum. To overcome this difficulty, some effective algorithms have been introduced: simulated annealing (SA)[1] and generalized-ensemble algorithms.[2—5] In this work, we employed Monte Carlo simulated annealing.

The other difficulty is how to include solvent effects: It is a non-trivial problem, because the number of solvent molecules that have to be considered is very large. Our method of including solvent effects is based on statistical mechanics. One of such approaches is RISM.[6,7] Recently, this algorithm has been used in simulations of protein folding.[8—10] This method is very powerful, but computationally demanding. The scaled particle theory[11,12] is another method based on the statistical mechanics of liquids, which is known to give good account of the hydration free energy of a non-polar solute.[12] The method requires much less computation time compared to the RISM method; thus, larger molecules can be treated. It has been successfully used to estimate the solvation free energy of biomolecules with a fixed conformation,[13,14] but has never been applied to simulations of protein folding. It is of great interest to apply this method to protein folding simulations and to examine the role which cavity-formation hydration plays in protein folding.

In the present work we combined Monte Carlo simulated annealing[1] and the extended scaled particle theory (ESPT).[13,14] We performed Monte Carlo simulated annealing simulations of Met-enkephalin in the gas phase and in aqueous solution, which is represented by the cavity-formation free energy. The simulations were repeated twenty times from randomly generated initial conformations, and the low-energy conformations were classified for both solvent environments.

Methods

Potential Energy Function. The energy function that we used in the present work is given by the sum of two terms: the conformational energy (E_P) of the protein molecule itself and the solvation free energy (ε_{SOL}) for the interaction of the protein with the surrounding solvent:

$$E_{TOT} = E_P + \varepsilon_{SOL}. \quad (1)$$

Here, note that solvation effects were included not by the solvation energy, but by the solvation free energy, because we wanted to estimate the average solvation effects for many configurations of water molecules around each fixed solute conformation. The conformational energy function (E_P, in kcal mol^{-1}) is given by the sum of the electrostatic term (E_C), the 12-6 Lennard–Jones term (E_{LJ}), and the hydrogen-bond term (E_{HB}) for all pairs of atoms in the molecule together with the torsion term (E_{TOR}) for all torsion angles:

$$E_P = E_C + E_{LJ} + E_{HB} + E_{TOR},$$
$$E_C = \sum_{(i,j)} \frac{332 q_i q_j}{\epsilon r_{ij}},$$
$$E_{LJ} = \sum_{(i,j)} \left(\frac{A_{ij}}{r_{ij}^{12}} - \frac{B_{ij}}{r_{ij}^{6}} \right),$$
$$E_{HB} = \sum_{(i,j)} \left(\frac{C_{ij}}{r_{ij}^{12}} - \frac{D_{ij}}{r_{ij}^{10}} \right),$$
$$E_{TOR} = \sum_i U_i \left(1 \pm \cos\left(n_i \chi^i \right) \right). \quad (2)$$

Here, r_{ij} is the distance (in Å) between atoms i and j, ϵ is the dielectric constant, and χ^i is the torsion angle for chemical bond i. Each atom is represented by a point at its center of mass, and the partial charge (q_i, in units of electronic charges) is assumed to be concentrated at that point. The factor 332 in E_C is a constant used to express the energy in units of kcal mol^{-1}. These parameters in the energy function as well as the molecular geometry were adopted from ECEPP/2.[15] The computer code KONF90[16,17] was used. The dielectric constant (ϵ) was set equal to 2. The peptide-bond dihedral angles (ω) were fixed at a value of 180° for simplicity. The remaining dihedral angles (ϕ and ψ) in the main chain and χ in the side chains thus constitute the variables to be updated in the simulations.

The solvation free energy of interactions between a solute molecule and solvent molecules can generally be divided into three contributions:

$$\varepsilon_{SOL} = \varepsilon_{CAV} + \varepsilon_{LJ} + \varepsilon_{EL}. \quad (3)$$

The first term is the cavity-formation term, which corresponds to the work required to create a cavity having the shape of the solute molecule in solution. The second term is the Lennard–Jones term between the solute and the solvent molecules. The third term is the electrostatic term (including the hydrogen-bond energy) between the solute and the solvent molecules.

The extended scaled particle theory[13,14] is used to calculate the cavity-formation term (ε_{CAV}) by scaling up a solute molecule in the solvent,

$$\varepsilon_{CAV} = W \qquad (\lambda = 1), \quad (4)$$

where λ is the scaling parameter, which varies from 0 (material point) to 1 (real size); $W(\lambda)$ is the work required to dissolve the scaled solute particle to the solvent. The theory assumes that $W(\lambda)$ can be represented for all positive values of λ by

$$W(\lambda) = A + B\lambda + \frac{1}{2} C\lambda^2 + PV_c(\lambda), \quad \lambda \geq 0, \quad (5)$$

where $V_c(\lambda)$ is the excluded volume of the scaled solute and P is the macroscopic pressure of the solvent. The term PV_c is very small for $\lambda = 1$ under a pressure of one atmosphere, and was neglected in the present work. The coefficients A, B, and C are determined using the continuity conditions up to second derivatives at $\lambda = 0$. The explicit expressions for A, B, and C are the following[14]:

$$A = -k_B T \ln(1 - \rho V_c(0)), \quad (6)$$

$$B = k_B T \frac{1}{1 - \rho V_c(0)} \rho \left(\frac{\partial V_c}{\partial \lambda} \right)_{\lambda=0}, \quad (7)$$

$$C = k_B T \frac{1}{1 - \rho V_c(0)} \rho \left(\frac{\partial^2 V_c}{\partial^2 \lambda} \right)_{\lambda=0} + k_B T \frac{1}{(1 - \rho V_c(0))^2} \rho^2 \left(\left(\frac{\partial V_c}{\partial \lambda} \right)_{\lambda=0} \right)^2, \quad (8)$$

where k_B is the Boltzmann constant, T is the absolute temperature, and ρ is the number density of the solvent molecules. The analytical evaluations of the excluded volume ($V_c(\lambda)$) and its derivatives were conducted using the code in Ref. 18. Together with the electrostatic interactions obtained by solving the Poisson–Boltzmann equations[19,20] and the Lennard–Jones interactions between the solute and the solvent, this theory can give a reasonable account for the solvation free energy (see Eq. 3). In this work, however, we included only the cavity-formation term for the solvation free energy, which has been used to model the hydrophobic free energy term.[21,22] Our interest here was how much variation of the conformations this cavity-formation term causes from those in gas phase, and we thus neglected other solvation terms.

Computational Details. For Met-enkephalin, whose amino-acid sequence is Tyr–Gly–Gly–Phe–Met, the number of degrees of freedom (namely, the number of dihedral angles to be updated) is 19. One Monte Carlo (MC) sweep consists of updating all 19 angles once with a Metropolis evaluation[23] for each update. In the present work, each SA run of Met-enkephalin consisted of 10000 MC sweeps with the initial temperature of 1000 K and the final temperature of 150 K. The temperature was lowered exponentially.[17] We made 40 SA runs altogether, starting from random initial conformations. Twenty SA runs were made for the simulations in the gas phase (namely, with only the conformational energy term (E_P)). The other twenty SA runs were simulations in the solvent (namely, with both the conformational energy term (E_P) and the cavity-formation free energy term (ε_{CAV})).

For the calculation of ε_{CAV}, which is based on ESPT, we used a constant temperature of 298.15 K for simplicity. The density of the water molecules was thus set equal to 1.0 g cm^{-3}. To calculate the excluded volumes, all hydrogen atoms in the system were regarded as being absorbed into the united atoms. The radii of all the united solute atoms were fixed to 1.9 Å for simplicity. That of the water molecule was taken to be 1.4 Å.

Results and Discussion

Ramachandran Plots. We first plot Ramachandran plots for the lowest-energy structures obtained by the present simulations. The results in the gas phase and in the solvent are shown in Fig. 1(a) and Fig. 1(b), respectively. The results for each individual residue are separately shown in Fig. 2. The distributions of points for the amino-acid residues, except for Gly, are limited mostly to the second and third quadrants ($\phi < 0$), while those for Gly are observed in all regions. This is in accord with the distributions obtained from a protein database, implying that our simulations were effective. From Figs. 1 and 2, we also find that the distributions of the dihedral angles in the gas phase are slightly more localized than those in the solvent. This seems to indicate that solvation tends to smooth out the free energy landscape of Met-enkephalin. However, the results in both cases are amazingly alike, and these Ramachandran plots cannot infer any definite conformational differences between the two cases.

Definition for Classification of Conformations. In order to compare the three-dimensional structures obtained by the present simulations in more detail, we calculated the root-mean-square distances (RMSD) between all pairs of the 40 lowest-energy conformations and four structures which were obtained in a previous work[24] as the characteristic con-

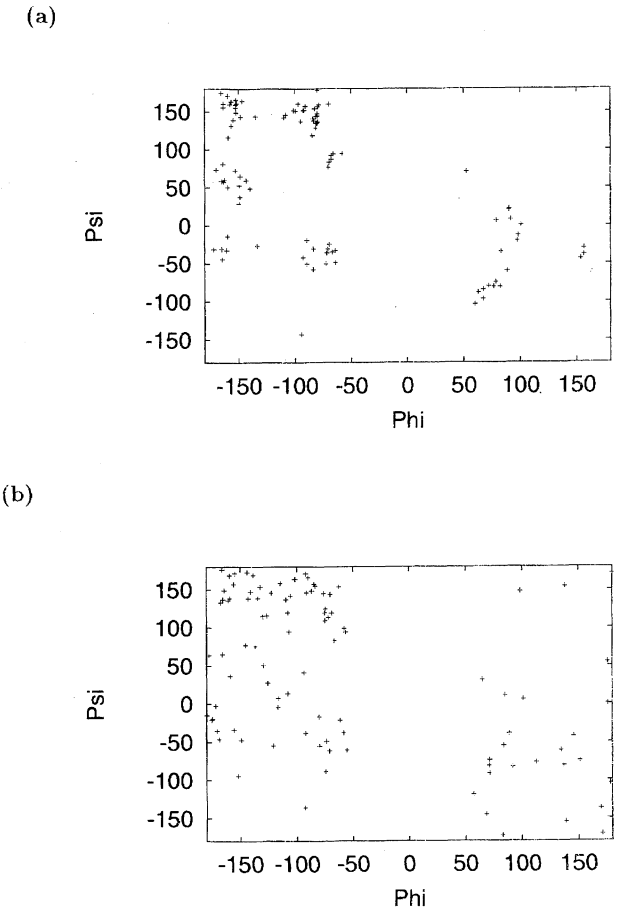

Fig. 1. Distribution of dihedral angles (ϕ, ψ) of the lowest-energy conformations of Met-enkephalin obtained in each of the 20 Monte Carlo simulated annealing runs in the gas phase (a) and in the solvent (b).

formations. We took into account only the atoms in the backbone. From these results, we classified the conformations into a few groups of similar structures. We define a group of conformations as follows.[17] Let W be the set of all conformations under consideration. A subset Y (with more than one conformation) of W is called a *group* of similar structures if it satisfies the following condition: For any conformation K in Y, there exists at least another conformation K′ in Y so that RMSD between conformations K and K′ is less than a cutoff c. (The definition depends on the value of c.) Each group corresponds to a specific tertiary structure and its small variations.

Detailed Results of Classification in Gas Phase. The RMSD in the gas phase are listed in Table 1. The conformations from column 2 to column 5 (A, B, C, and D) are the lowest-energy structures obtained previously in the gas phase, which represent the four groups found in Ref. 24. The other 20 conformations (V1, V2, ⋯, and V20) are the lowest-energy structures obtained by the present simulations in the gas phase. The numbers enclosed in the solid lines, and the dashed lines in Table 1 indicate that the corresponding pairs of conformations form a group of similar structures with the cutoff $c = 1.0$ Å and $c = 1.5$ Å, respectively. We thus have, respectively, six groups (six boxes in solid lines) and three groups (three boxes in dashed lines) for the two cutoff values. The numbers in bold in Table 1 from the second to the fifth column are the entries that are less than or equal to 1.0. These entries imply that the group which includes conformations V1, V2, and V3 has similar structures to A. Likewise, the group which includes conformations V6, V7, and V8 has similar structures to D, and that including V10 and V11 to B. Hence, we refer to these three groups as groups A_1 (including V1,V2, and V3), D_1 (including V6, V7, and V8), and B_1 (including V10 and V11) (as defined with cutoff $c = 1.0$ Å). Furthermore, the underlined numbers in Table 1 indicate that they are more than 1.0 and less than or equal to 1.5. These entries imply that conformations V13, V14, V17, and V18 have similar structures to group B. We thus refer to the group including V13, V14, V15, and V16 as B_1' and that including V17 and V18 as B_1'' (as defined with cutoff $c = 1.0$ Å). The remaining group was named E_1 (including V19 and V20). With the cutoff $c = 1.5$ Å, it is found that conformation V4 and those of group A_1 form a single group, which we refer to as group A_2 and that conformations V9 and V12 and those of groups D_1, B_1, B_1', and B_1'' constitute a single group, which we refer to as group B_2. All these results of classifications are listed in Table 2.

We now summarize the main features in the results of the classification. The lowest-energy conformation obtained throughout the present simulations (global-minimum-energy structure) is essentially identical with that obtained in previous simulations[24,25] and belongs to group A_1. Groups A_2 and B_2 are dominant in the gas phase. Group D_1 represents an intermediate structure between group A_1 and group B_1.

After the classification of the conformations into groups of similar structures is finished, we now examine the structural characterizations of each group in detail. Here, we only consider conformations of the six groups (A_1, D_1, B_1, B_1', B_1'', and E_1 in Table 2) obtained with the cutoff $c = 1.0$ Å. In Fig. 3 we show the lowest-energy conformations (left-hand side) and the superposed backbone structures of all conformations (right-hand side) in each group.

As can be seen in Fig. 3(a), the structures in group A_1 have two hydrogen bonds between the amide nitrogen of Gly-2 and the carbonyl oxygen of Met-5 backbone and between the carbonyl oxygen of Gly-2 and the amide nitrogen of Met-5 backbone. This structure is actually a type II′ β-turn involving the residues Gly–Gly–Phe–Met. Moreover, OH in the Tyr-1 side chain is hydrogen-bonded to the carbonyl oxygen of the Gly-3 backbone. It was found that the side-chain structures of Tyr-1 and Met-5 are very stable, while that of Phe-4 is slightly more flexible. The structure of group A_1 is very stable, because of these intrachain hydrogen bonds. For instance, the conformations in group A_1 are more similar to each other than those in the other groups (RMSD are as small as 0.3 Å in Table 1).

As can be seen in Fig. 3(b), the structures in group B_1 have two hydrogen bonds between the amide nitrogen of Tyr-1 and the carbonyl oxygen of Phe-4 and between the carbonyl oxygen of Tyr-1 and the amide nitrogen of Phe-4 backbone. This

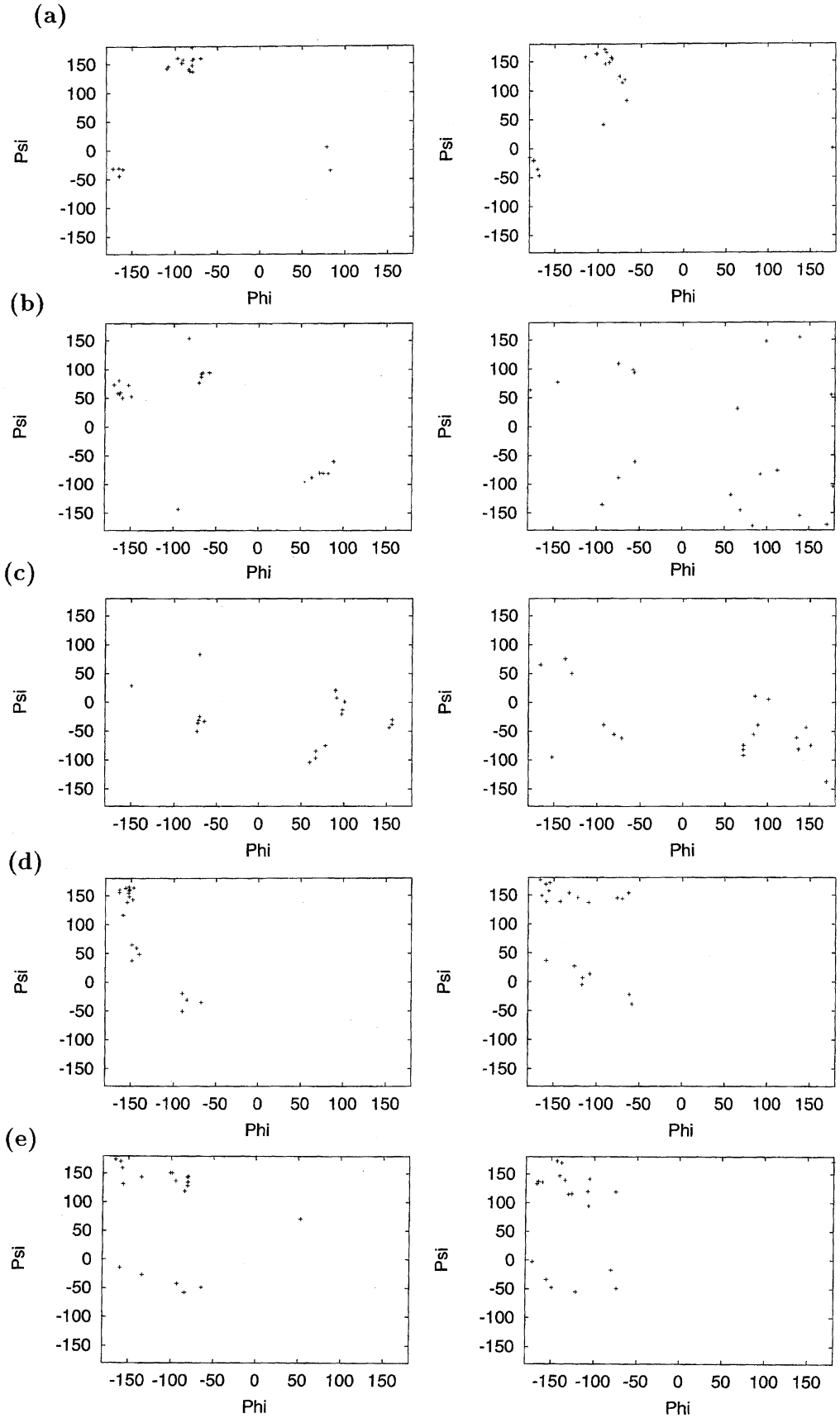

Fig. 2. Distribution of dihedral angles of the lowest-energy conformations of Met-enkephalin for Tyr-1 (a), Gly-2 (b), Gly-3 (c), Phe-4 (d), and Met-5 (e), which were obtained by the 20 Monte Carlo simulated annealing simulations in the gas phase (left-hand side) and in the solvent (right-hand side).

Table 1. The Root-Mean-Square Distances (Å) among Pairs of the Twenty Lowest-Energy Conformations Obtained by Monte Calro Simulated Annealing Simulations in Gas Phase[a)]

	A	C	B	D	V1	V2	V3	V4	V5	V6	V7	V8	V9	V10	V11	V12	V13	V14	V15	V16	V17	V18	V19	V20
V1	**0.2**	2.3	2.7	1.7		0.3	0.3	1.1	2.0	1.9	1.9	2.0	2.3	2.5	2.6	2.6	2.7	2.7	2.7	2.7	2.8	2.6	2.8	2.8
V2	**0.2**	2.2	2.6	1.7	0.3		0.3	1.2	1.9	1.9	1.8	1.9	2.2	2.5	2.5	2.5	2.6	2.6	2.6	2.6	2.7	2.6	2.8	2.8
V3	**0.2**	2.2	2.6	1.7	0.3	0.3		1.1	1.9	1.9	1.8	1.9	2.2	2.4	2.5	2.5	2.6	2.6	2.6	2.6	2.7	2.6	2.8	2.9
V4	1.1	2.3	2.6	1.7	1.1	1.2	1.1		2.1	1.9	1.8	1.9	2.0	2.4	2.6	2.4	2.5	2.6	2.6	2.5	2.8	2.7	2.8	2.9
V5	2.0	1.7	1.7	1.8	2.0	1.9	1.9	2.1		1.7	1.7	1.6	1.8	1.6	1.7	2.1	1.9	1.9	2.0	2.0	2.0	1.9	2.7	2.8
V6	1.9	2.5	1.6	**0.9**	1.9	1.9	1.9	1.9	1.7		0.7	0.9	1.4	1.6	1.8	1.8	1.8	1.9	2.0	2.0	1.8	1.8	2.2	2.5
V7	1.8	2.5	1.8	**0.7**	1.9	1.8	1.8	1.8	1.7	0.7		0.7	1.3	1.4	1.7	1.7	1.9	2.0	1.9	1.9	2.0	1.9	2.5	2.6
V8	1.9	2.3	1.7	**0.8**	2.0	1.9	1.9	1.9	1.6	0.9	0.7		1.2	1.4	1.6	1.4	1.8	1.9	1.8	1.8	1.8	1.7	2.4	2.5
V9	2.2	2.1	1.5	1.4	2.3	2.2	2.2	2.0	1.8	1.4	1.3	1.2		1.2	1.5	1.2	1.7	1.7	1.6	1.7	1.8	1.7	2.5	2.6
V10	2.5	1.9	**1.0**	1.6	2.5	2.5	2.4	2.4	1.6	1.6	1.4	1.4	1.3		0.9	1.4	1.6	1.7	1.6	1.7	1.7	1.6	2.7	2.9
V11	2.6	2.0	**0.7**	1.8	2.6	2.5	2.5	2.6	1.7	1.8	1.7	1.6	1.5	0.9		1.4	1.4	1.5	1.4	1.5	1.5	1.5	2.5	2.5
V12	2.6	2.1	1.5	1.6	2.6	2.5	2.5	2.4	2.1	1.8	1.7	1.4	1.2	1.4	1.4		1.7	1.7	1.6	1.6	1.4	1.3	2.3	2.4
V13	2.6	2.2	1.2	1.9	2.7	2.6	2.6	2.5	1.9	1.8	1.9	1.8	1.7	1.6	1.4	1.7		0.9	1.1	1.2	1.7	1.7	2.4	2.6
V14	2.7	2.1	1.4	2.0	2.7	2.6	2.6	2.6	1.9	1.9	2.0	1.9	1.7	1.7	1.5	1.7	0.9		0.7	0.7	1.5	1.4	2.7	2.9
V15	2.6	2.1	1.6	1.9	2.7	2.6	2.6	2.6	2.0	2.0	1.9	1.8	1.6	1.6	1.4	1.6	1.1	0.7		0.3	1.7	1.6	2.8	2.9
V16	2.6	2.0	1.7	2.0	2.7	2.6	2.6	2.5	2.0	2.0	1.9	1.8	1.7	1.7	1.5	1.6	1.2	0.7	0.3		1.7	1.5	2.9	3.0
V17	2.8	2.1	1.3	2.0	2.8	2.7	2.7	2.8	2.0	1.8	2.0	1.8	1.8	1.7	1.5	1.4	1.7	1.5	1.7	1.7		0.4	2.1	2.3
V18	2.8	1.9	1.3	1.9	2.6	2.6	2.6	2.7	1.9	1.8	1.9	1.7	1.7	1.6	1.5	1.3	1.7	1.4	1.6	1.5	0.4		2.3	2.5
V19	2.8	3.0	2.3	2.2	2.8	2.8	2.8	2.8	2.7	2.2	2.5	2.4	2.5	2.7	2.5	2.3	2.4	2.7	2.8	2.9	2.1	2.3		0.8
V20	2.8	3.1	2.5	2.3	2.8	2.8	2.9	2.9	2.8	2.5	2.6	2.5	2.6	2.9	2.5	2.4	2.6	2.9	2.9		2.3	2.5	0.8	

a) Conformations from column 2 to column 5 correspond to the lowest-energy conformations in groups A, B, C, and D obtained by previous simulations.[24] The other 20 conformations (V1,V2, ···, and V20) correspond to the lowest-energy conformations obtained by the present simulations in gas phase. The numbers enclosed in solid lines and dashed lines indicate that the corresponding conformations form a group of similar structures with the cutoff c = 1.0 Å and c = 1.5 Å, respectively. The numbers in bold from the second to the fifth column are the entries that are less than or equal to 1.0. The underlined numbers indicate that they are more than 1.0 and less than or equal to 1.5.

Table 2. The Results of Classification of the Lowest-Energy Conformations Obtained by the Present Simulations in Gas Phase

c[a] (Å)	Group	n[b]	Lowest-energy[c] (kcal mol^{-1})
1.0	$A_1 = \{1,2,3\}$	3	−11.2
	$D_1 = \{6,7,8\}$	3	−7.3
	$B_1 = \{10,11\}$	2	−9.7
	$B_1' = \{13,14,15,16\}$	4	−7.2
	$B_1'' = \{17,18\}$	2	−7.0
	$E_1 = \{19,20\}$	2	−8.2
1.5	$A_2 = \{4\} \cup A_1$	4	−11.2
	$B_2 = \{9,12\} \cup D_1 \cup B_1 \cup B_1' \cup B_1''$	13	−9.7
	$E_2 = E_1$	2	−8.2

a) c is the cutoff value. b) n is the number of structures in each group. c) In the fourth column we list the lowest-energy value in each group.

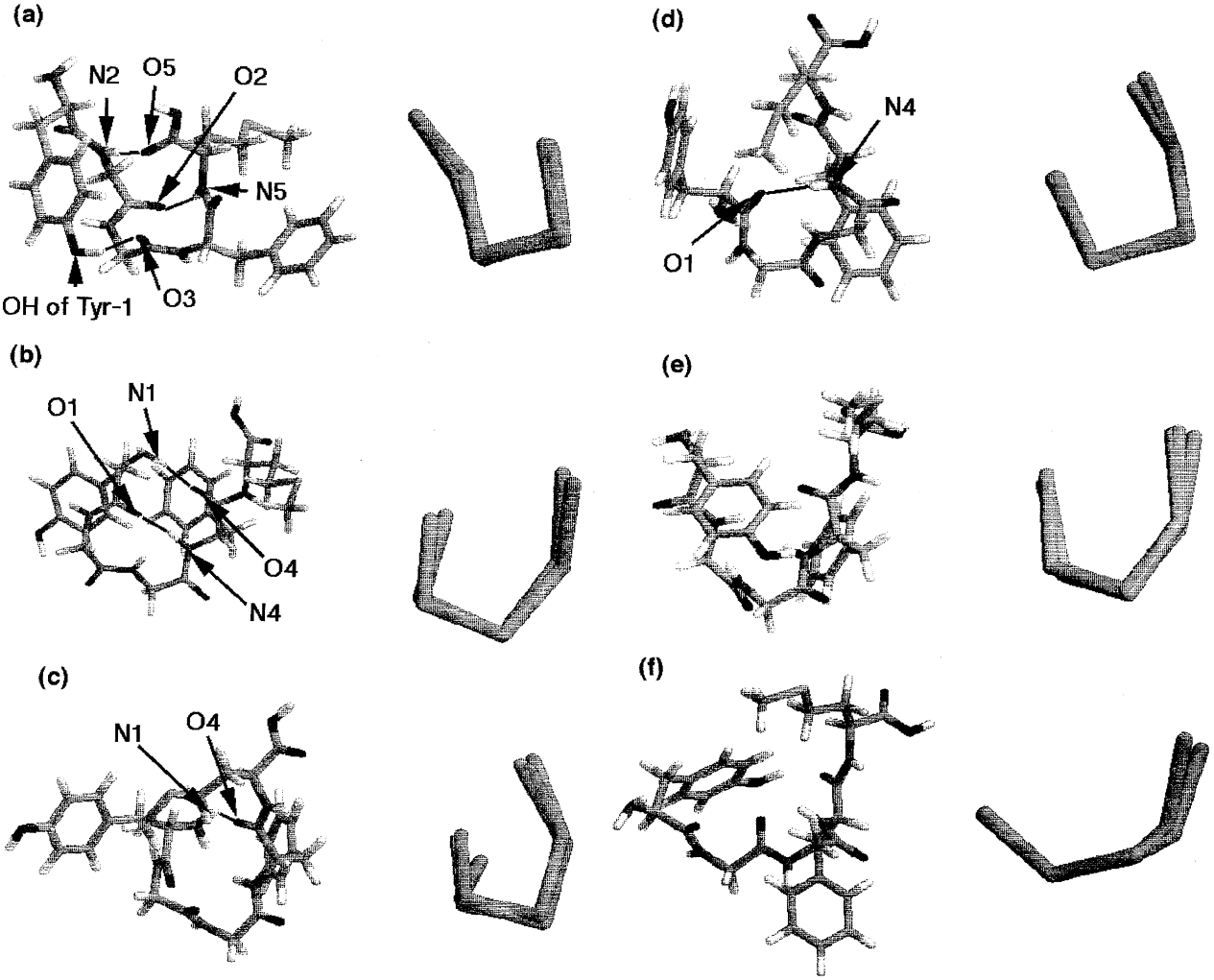

Fig. 3. The structural characterization of groups A_1, D_1, B_1, B_1', B_1'', and E_1 (from Table 2) obtained by Monte Carlo simulated annealing simulations in the gas phase. The left-hand side is the lowest-energy conformation in each group, and the right-hand side is the superposition of the backbone structures of all the conformations in each group. (a) Group A_1 (Conformation V1 in Table 1). (b) Group B_1 (Conformation V10 in Table 1). (c) Group B_1' (Conformation V13 in Table 1). (d) Group B_1'' (Conformation V17 in Table 1). (e) Group D_1 (Conformation V6 in Table 1). (f) Group E_1 (Conformation V19 in Table 1). We use a simplified notation such as O2 and N5, which stand for the carbonyl oxygen of the Gly-2 backbone and the amide nitrogen of the Met-5 backbone, respectively. The figures were created with Ras Mol.[26]

structure is actually a type II β-turn involving the residues Tyr–Gly–Gly–Phe. These structures are also stable, because they have two intrachain hydrogen bonds and this group has the second-lowest energy among the six groups (group A_1

has the global-minimum energy).

The main-chain structures of groups B_1' and B_1'' are similar to those of group B_1, as can be seen in Figs. 3(c) and 3(d). The structures in these groups are slightly distorted from those in group B_1 in the sense that they have only one of the two intrachain hydrogen bonds of group B_1 formed. Group B_1' has only one hydrogen bond between the amide nitrogen of Tyr-1 and the carbonyl oxygen of Phe-4, and B_1'' has a hydrogen bond between the carbonyl oxygen of Tyr-1 and the amide nitrogen of Phe-4. These structures have slightly higher energies than those of group B_1. Also note that the side-chain structures are more deviated compared to the backbone.

As can be seen in Fig. 3(e), group D_1 has intermediate structures between group A_1 and B_1. This group has a hydrogen bond between the carbonyl oxygen of Gly-2 and the amide nitrogen of Phe-4, and forms a γ turn. As in the case for group A_1, OH in the Tyr-1 side chain is hydrogen-bonded to the carbonyl oxygen of the Gly-3 backbone, and the side-chain structure of Tyr-1 is stable. Group D_1 has a considerably higher energy than groups A_1 and B_1.

In group E_1 (Fig. 3(f)), the main chain is more extended than that of the other groups. There is no intrachain hydrogen bond in the backbone. There is a hydrogen bond between OH of the Tyr-1 side chain and the carbonyl oxygen of the Phe-4 backbone, which seems to stabilize the structure.

In summary, we found that groups A and B are dominant and stable in the gas phase (they correspond to the global-minimum-energy state and the second-lowest-energy state, respectively). These structures are stabilized by two intrachain backbone hydrogen bonds. As is shown in Tables 1 and 2, however, the number of obtained structures of group B (including B_1' and B_1'') is larger than that of group A.

Detailed Results of Classification in Solvent. We now present the results of simulations in the solvent. In Table 3, the RMSD in the solvent are listed. The conformations from column 2 to column 7 correspond to the lowest-energy conformations in groups A_1, D_1, B_1, B_1', B_1'', and E_1 obtained by the present simulations in the gas phase, and actually are V1, V10, V13, V17, V6, and V19 in Table 1, respectively. The other 20 conformations (S1, S2, $\cdots$, and S20) are the lowest-energy conformations obtained by the present simulations in the solvent. The numbers enclosed in solid lines and dashed lines in Table 3 indicate that the corresponding conformations form a group of similar structures with the cutoff $c = 1.0$ Å and $c = 1.5$ Å, respectively. We thus have three groups (boxes in solid line and dashed line) for the two cutoff values. The numbers in bold in Table 3 from the second to the seventh column are those entries that are less than or equal to 1.0. These entries imply that conformations S4 and S5 have similar structures to B_1. Hence, we refer to the group including S4, S5, and S6 as group B_3 (as defined with cutoff $c = 1.0$ Å). Furthermore, the underlined numbers in Table 3 indicate that they are more than 1.0 and less than or equal to 1.5. These entries imply that the group which includes conformations S1 and S2 have intermediate structures between B_1 and D_1. We refer to the group including S1 and S2 as group B_3' (as defined with cutoff $c = 1.0$ Å). The remaining group including S9 and S10 was named F_3. As for the classifications of groups having similar structures with the cutoff $c = 1.5$ Å (boxes in dashed lines), it is found that conformations S3, S7, S8, S11, and S12 and groups B_3', B_3, and F_3 form a single group, which we refer to as group B_4, and that conformations S14, S15, and S16 constitute a single group, which we refer to as group G_4. The remaining group includes S17, S18, and S19, which we refer to as group E_4, because two of the entries in this group are less than 1.5 Å from group E_1. We thus find that for $c = 1.5$ Å, there are three groups (B_4, G_4, and E_4). All of these results of classifications are summarized in Table 4. We remark that the lowest-energy conformation obtained throughout the present simulations (global-minimum-energy structure) belongs to group B_3' (Conformation S1). In the case of the cutoff $c = 1.5$ Å, this structure belongs to the main group B_4.

After the classification of conformations into groups of similar structures is finished, we now examine the structural characterizations of each group in detail. In Fig. 4 we show the lowest-energy conformations (left-hand side) and the superposed backbone structures of all conformations (right-hand side) in each group. As can been seen in Fig. 4(a), the structures in group B_3' have a hydrogen bond between the amide nitrogen of Tyr-1 and the carbonyl oxygen of the Phe-4 backbone. Moreover, the side-chain of Tyr-1 is close to that of Met-5. As can be seen in Fig. 4(b), the structures in group B_3 have two hydrogen bonds between the amide nitrogen of Tyr-1 and the carbonyl oxygen of Phe-4 and between the carbonyl oxygen of Tyr-1 and the amide nitrogen of Phe-4. The structures of group B_3 actually form a type II β-turn involving the residues Tyr–Gly–Gly–Phe. These structures are very similar to those in group B in gas phase. The structures in group F_3 (Fig. 4(c)) do not have any intrachain hydrogen bonds. However, the shape of the main chain is similar to that of group B in the gas phase.

In groups G_4 and E_4 (Figs. 4(d) and 4(e)), obtained with the cutoff $c = 1.5$ Å, the main chain is more extended than that of the other groups. There is no intrachain hydrogen bond in the backbone. However, the structures in these groups form a circular shape in which the main chain is extended, but the side chain of Tyr-1 is close to the that of Met-5.

We now summarize the main features in the results of the classification. Two characteristic conformations were found from the present simulations in solvent. First, the backbone structure of many conformations is similar to that in group B obtained in the gas phase. (The structures in group B have a hydrogen bond between the amide nitrogen of Tyr-1 and the carbonyl oxygen of Phe-4 backbone.) In the other set of conformations, the side chain of Tyr-1 tends to be close to that of Met-5, forming a circular shape as a whole, while the backbone is extended. The main-chain conformations are similar to those of group E_1 obtained in the gas phase. These facts imply that the backbone structures obtained by simulations in the solvent do not differ significantly from those in the gas phase. The side-chain structures, however, can be quite different. For instance, the lowest-energy conforma-

Table 3. The Root-Mean-Square Distances (Å) among Pairs of the Twenty Lowest-Energy Conformations Obtained by Monte Calro Simulated Annealing Simulations in Solvent[a)]

	A_1	D_1	B_1	B_1'	B_1''	E_1	S1	S2	S3	S4	S5	S6	S7	S8	S9	S10	S11	S12	S13	S14	S15	S16	S17	S18	S19	S20
TOT	36.4	38	38.6	39	37.5	38.5	23.7	26.5	29.8	35.9	31.7	26.1	25.7	31	33.5	33.8	33.9	37.9	35.3	29.2	31.2	33.4	30.6	27.5	33.5	33.3
SOL	47.6	45.3	48.3	46.2	44.5	46.8	24.6	27.9	26.2	40.3	40	27.9	24.4	39.6	40.7	41.1	32.4	31	37.3	32.3	25.4	27.2	26.2	22.5	27.6	31.6
GAS	−11.2	−7.3	−9.7	−7.2	−7	−8.3	−0.9	−1.4	3.6	−4.4	−8.3	−1.8	1.3	−8.6	−7.2	−7.3	1.5	6.9	−2.0	−3.1	5.8	6.2	4.4	5.0	5.9	1.7
S1	2.4	1.1	1.3	1.7	1.6	2.4		0.8	1.4	1.4	1.1	1.9	1.5	1.5	1.8	2.0	2.6	2.4	2.0	2.6	3.0	2.7	3.0	2.7	3.0	2.5
S2	2.4	1.3	1.3	1.5	1.7	2.5	0.8		1.2	1.4	1.3	1.9	1.4	1.3	1.8	2.0	2.6	2.4	1.9	2.7	3.0	2.7	3.0	2.7	2.9	2.5
S3	2.3	1.6	1.3	1.9	2.0	2.5	1.4	1.2		1.3	1.4	1.7	1.8	1.1	1.7	1.8	2.4	2.3	2.3	2.9	2.9	2.7	3.0	2.9	2.9	2.5
S4	2.6	1.5	**1.0**	1.9	1.7	2.2	1.4	1.4	1.3		1.0	1.0	1.8	1.5	1.6	1.6	2.4	2.0	2.1	3.0	2.9	2.8	2.9	2.8	2.8	2.3
S5	2.7	1.6	**0.9**	1.5	1.4	2.4	1.1	1.3	1.4	1.0		1.5	1.5	1.8	1.5	1.8	2.6	2.4	2.1	2.6	3.0	2.7	3.0	2.7	2.8	2.3
S6	2.6	1.8	1.6	2.2	1.9	1.9	1.9	1.9	1.7	1.0	1.5		2.2	1.6	1.8	1.6	2.0	1.8	1.8	2.8	2.3	2.4	2.4	2.5	2.3	2.0
S7	2.5	1.6	1.5	**0.9**	1.7	2.8	1.5	1.4	1.8	1.8	1.5	2.2		2.0	1.8	2.0	3.1	2.8	2.1	2.4	3.1	2.8	3.0	2.4	3.0	2.4
S8	2.0	1.4	1.7	2.1	2.2	2.1	1.5	1.3	1.1	1.5	1.8	1.6	2.0		1.8	1.7	2.2	1.9	1.8	2.7	2.5	2.4	2.6	2.6	2.6	2.3
S9	2.3	1.7	1.7	1.8	1.9	2.2	1.8	1.8	1.7	1.6	1.5	1.8	1.8	1.8		0.8	2.2	1.9	2.0	2.6	2.6	2.5	2.5	2.4	2.4	2.1
S10	2.2	1.8	2.0	2.1	2.1	2.1	2.0	2.0	1.8	1.6	1.8	1.6	2.0	1.7	0.8		1.9	1.5	2.1	2.7	2.4	2.3	2.3	2.4	2.1	1.9
S11	2.9	2.4	2.9	3.1	2.6	1.7	2.6	2.6	2.4	2.4	2.6	2.0	3.1	2.2	2.2	1.9		1.4	2.1	3.0	1.9	2.1	2.0	2.5	2.0	2.4
S12	2.7	2.1	2.6	2.8	2.5	1.8	2.4	2.4	2.3	2.0	2.4	1.8	2.8	1.9	1.9	1.5	1.4		2.2	3.1	2.4	2.5	2.0	2.5	2.2	2.6
S13	2.4	1.8	2.2	1.9	1.8	1.7	2.0	1.9	2.3	2.1	2.1	1.8	2.1	1.8	2.0	2.1	2.1	2.2		2.0	2.2	1.9	2.0	1.7	2.1	2.0
S14	2.0	2.5	2.7	2.4	2.2	2.6	2.6	2.7	2.9	3.0	2.6	2.8	2.4	2.7	2.6	2.7	3.0	3.1	2.0		2.1	1.4	2.3	1.7	2.5	1.9
S15	2.4	2.8	3.1	3.2	2.7	1.9	3.0	3.0	2.9	2.9	3.0	2.3	3.1	2.5	2.6	2.4	1.9	2.4	2.2	2.1		1.4	1.8	2.1	1.8	1.8
S16	2.2	2.5	2.8	2.8	2.4	1.9	2.7	2.7	2.7	2.8	2.7	2.4	2.8	2.4	2.5	2.3	2.1	2.5	1.9	1.4	1.4		1.7	1.8	2.0	1.6
S17	2.7	2.8	3.2	3.0	2.6	1.4	3.0	3.0	3.0	2.9	3.0	2.4	3.0	2.6	2.5	2.3	2.0	2.0	2.0	2.3	1.8	1.7		1.3	1.1	2.2
S18	2.6	2.6	2.9	2.3	2.1	1.7	2.7	2.7	2.9	2.8	2.7	2.5	2.4	2.6	2.4	2.4	2.5	2.5	1.7	1.7	2.1	1.8	1.3		1.4	2.1
S19	2.9	2.8	3.1	2.9	2.4	1.4	3.0	2.9	2.9	2.8	2.8	2.3	3.0	2.6	2.4	2.1	2.0	2.2	2.1	2.5	1.8	2.0	1.1	1.4		2.1
S20	1.9	2.3	2.4	2.4	2.5	2.3	2.5	2.5	2.5	2.3	2.3	2.0	2.4	2.3	2.1	1.9	2.4	2.6	2.0	1.9	1.8	1.6	2.2	2.1	2.1	

a) Conformations from column 2 to column 7 correspond to the lowest-energy conformations in groups A_1, D_1, B_1, B_1', B_1'', and E_1 obtained by the present simulations in gas phase and actually are V1, V10, V13, V17, V6, and V19 in Table 1, respectively. The other 20 conformations (S1, S2, ⋯, and S20) correspond to the lowest-energy conformations obtained by the present simulations in solvent. The numbers enclosed in solid lines and dashed lines indicate that the corresponding conformations from a group of similar structures with the cutoff c = 1.0 Å and c = 1.5 Å, respectively. The numbers in bold from the second to the seventh column are the entries that are less than or equal to 1.0. The underlined numbers indicate that they are more than 1.0 and less than or equal to 1.5.

Table 4. The Results of Classification of the Lowest-Energy Conformations Obtained by the Present Simulations in Solvent

$c^{a)}$ (Å)	Group	$n^{b)}$	Lowest-energy$^{c)}$ (kcal mol^{-1})
1.0	$B_3' = \{1,2\}$	2	23.7
	$B_3 = \{4,5,6\}$	3	26.1
	$F_3 = \{9,10\}$	2	33.5
1.5	$B_4 = \{3,7,8,11,12,13\} \cup B_3' \cup B_3 \cup F_3$	13	23.7
	$G_4 = \{14,15,16\}$	3	29.2
	$E_4 = \{17,18,19\}$	3	27.5

a) c is the cutoff value. b) n is the number of structures in each group. c) In the fourth column we list the lowest-energy value in each group.

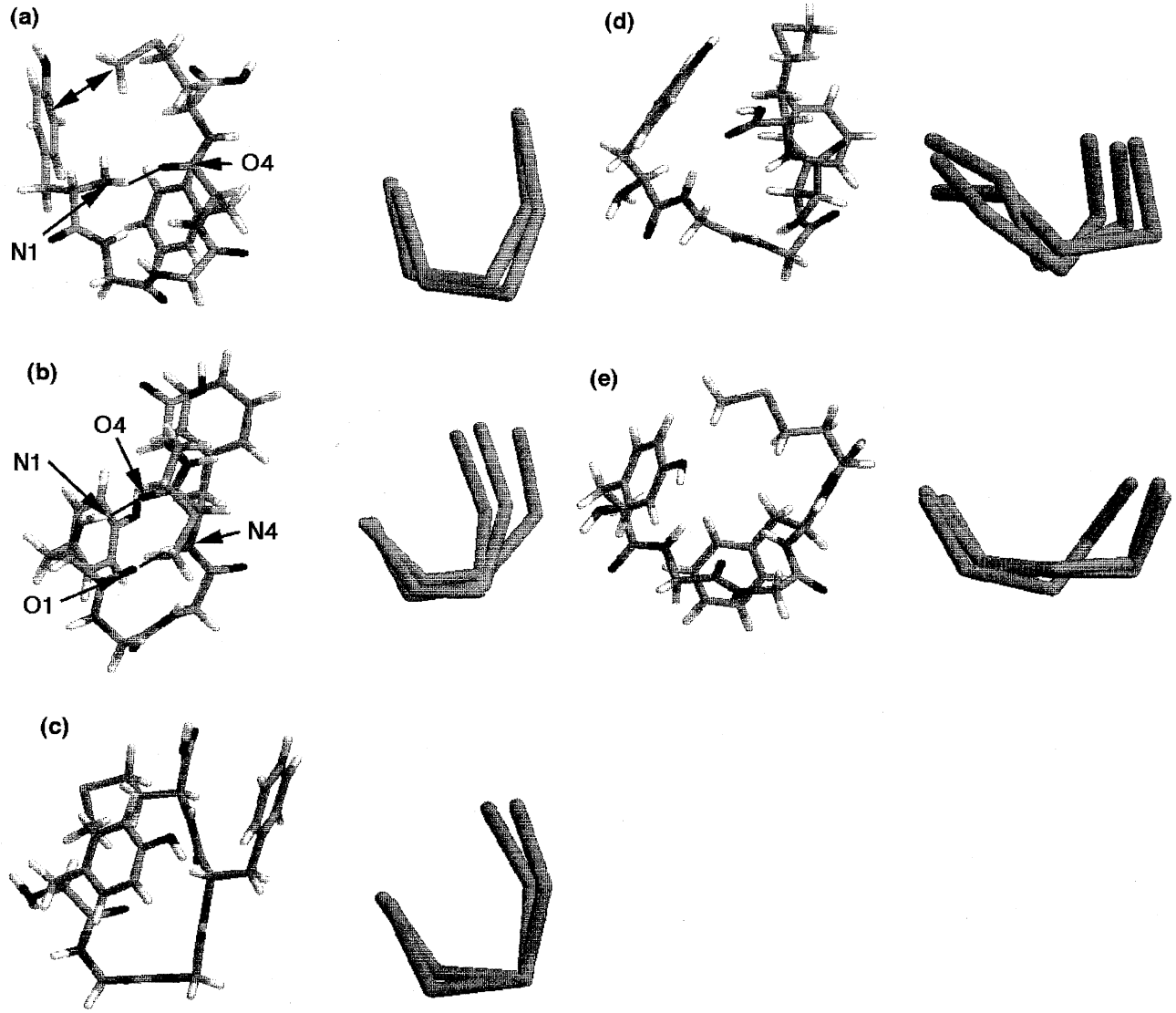

Fig. 4. The structural characterization of groups B_3', B_3, F_3, G_4, and E_4 (from Table 4) obtained by Monte Carlo simulated annealing simulations in the solvent. The left-hand side is the lowest-energy conformation in each group, and the right-hand side is the superposition of the backbone structures of all the conformations in each group. (a) Group B_3' (Conformation S1 in Table 4). (b) Group B_3 (Conformation S6 in Table 4). (c) Group F_3 (Conformation S5 in Table 4). (d) Group G_4 (Conformation S14 in Table 4). (e) Group E_4 (Conformation S18 in Table 4). We use a simplified notation such as O2 and N5, which stand for the carbonyl oxygen of the Gly-2 backbone and the amide nitrogen of the Met-5 backbone, respectively. The figures were created with Ras Mol.[26]

tion in group B_1 (Fig. 3(b)) and that in group B_3' (Fig. 4(a)) have very similar backbone structures (RMSD = 1.3 Å) but completely different side-chain orientations. Also note that the global-minimum-energy structure in the gas phase (group A_2) has a rather higher energy in solution, and is not found by the present simulations including a solvent.

Characteristics of the Lowest-Energy Conformations Obtained in Gas Phase and in Model Solvent. The total energy (E_{TOT}) used in the present simulations was

$$E_{TOT} = E_P \tag{9}$$

for the gas-phase case and

$$E_{TOT} = E_P + \varepsilon_{CAV} \tag{10}$$

for the in-solvent case, where E_P is the conformational energy (see Eq. 2) and ε_{CAV} is the cavity-formation term (see Eqs. 4 and 5). In order to see how stable the low-energy conformations in the gas phase are when they are placed in the solvent, we calculated the cavity-formation term (ε_{CAV}) for six conformations (A_1, D_1, B_1, B_1', B_1'', and E_1) and list the values in Table 3 (see the third row in the table). As can be seen from Table 3, these cavity-formation terms are significantly larger than those of conformations (S1, S2, ⋯, and S20) obtained by simulations in the solvent, suggesting that these gas-phase conformations are unstable in the solvent. Note that the entries in Table 3 are the root-mean-square distances of the backbone structure only. The fact that some of the values between the conformations in the gas phase and those in the solvent are small (see the entries in bold face and underlined numbers) seems to imply that when the low-energy conformations in the gas phase are placed in the solvent, they rearrange the side-chain orientations so that the backbone structures remain stable. An exception is the conformation in group A_1. The side-chain structures (especially that of Tyr-1) are also constrained for these conformations so that they cannot be rearranged to find a stable conformation in the solvent. The backbone of the lowest-energy structure in the solvent has a shape similar to that of the second lowest-energy structure in gas phase; the global-minimum-energy conformation in the gas phase was not found in the simulations in the solvent. Furthermore, as can be seen from Tables 2 and 4, the energy difference between the lowest-energy group and the second lowest-energy group is 1.5 kcal mol^{-1} in the gas phase (A_2 versus B_2) and 3.8 kcal mol^{-1} and in the solvent (B_4 versus H_4), respectively. Therefore, there is only one dominant low-energy structure in the slovent, while there are two dominant ones in the gas phase. It seems that the solvent effects decrease the number of low-energy local minima.

We now focus our attention on the conformations obtained in the solvent which have a low cavity-formation free energy (ε_{CAV}). These are conformations S1, S2, S3, S6, S7, S15, S16, S17, S18, and S19 (see Table 3). By examining the structures in detail, we found two characteristics. One is that the conformations with a hydrogen bond between the amide nitrogen of Tyr-1 and the carbonyl oxygen of Phe-4 backbone have low cavity-formation free energies. These conformations are S1, S2, S3, and S7, which are shown in Fig. 5(a). The other is that the conformations have low cavity-formation free energies when they form a circular shape in which the N-terminal side chain (Tyr-1) is close to the C-terminal one (Met-5) and the main chain is extended. These conformations are S6, S15, S16, S17, S18, and S19, which are shown in Fig. 5(b).

In Fig. 6, cavity-formation free energy of the lowest-energy conformations obtained by each simulation in the solvent as a function of the accessible surface area is shown. The accessible surface areas of the obtained conformations were calculated by the code developed in Ref. 18. It is found that there are two parts in Fig. 6. One part (Part 1) corresponds to the structures that have high cavity-formation free energies and small accessible surface areas. These conformations are similar to those of group B in the gas phase, which have two intrachain hydrogen bonds and have low conformational energies. In this case, the conformational energies are responsible for the conformational stability in the solvent. On the other hand, the second part (Part 2) in Fig. 6 corresponds to the structures that have low cavity-formation free energies and large accessible surface areas. These structures have either circular shapes in which the main chain is extended, but the N-terminal side chain (Tyr-1) is close to the C-terminal one (Met-5), or have a hydrogen bond between the amide nitrogen of Tyr-1 and the carbonyl oxygen of Phe-4 (one of the hydrogen bonds of group B is broken). In this case, the cavity-formation free energy is responsible for the conformational stability in the solvent.

Relation between the Cavity-Formation Free Energy and the Accessible Surface Area. We now consider in detail the relations among the solvent-accessible surface area, the solvent-excluded volume, and the cavity-formation free energy. We performed three SA runs of 10000 MC sweeps in the model solvent with the initial temperature of 1000 K and the final temperature of 150 K. One of the simulation runs, which we refer to as Run 1, was made so that it reproduces the one that gave the lowest-energy conformation in Part 1 of Fig. 6. Another run (Run 2) reproduces the lowest-energy conformation in Part 2 of Fig. 6. The third run (Run 3) was newly made. One conformation at each temperature with an increment of 1 degree (T = 150, 151, 152, ⋯, and 1000 K) was chosen for the analyses (total of 851 conformations for each run). In Fig. 7, we show the solvent-excluded volume of these conformations as a function of their accessible surface area. The excluded volumes of these conformations were calculated by the code developed in Ref. 18. It was found that the excluded volume is almost proportional to the accessible surface area. In Fig. 8, the cavity-formation free energies of the conformations as a function of the accessible surface area are shown. In Fig. 8(a), the data from all 851×3 conformations are shown. The data in Fig. 8(b) and Fig. 8(c) are from the conformations which have $E_{TOT} < 40$ kcal mol^{-1} in Run 1 and Run 2, respectively (the results of Run 3 are omitted because they turned out to be similar to those of Run 2). From Fig. 8, it is found that the low-energy conformations obtained in these simulations remain in Part 1 or Part 2 of Fig. 6. Figure 8(b) implies that the cavity-formation free energy of the lower-energy conformations ($E_{TOT} < 40$ kcal mol^{-1}) in Run 1 is proportional to the accessible surface area. On the other hand, Fig. 8(c) suggests that the cavity-formation free energy of low-energy confor-

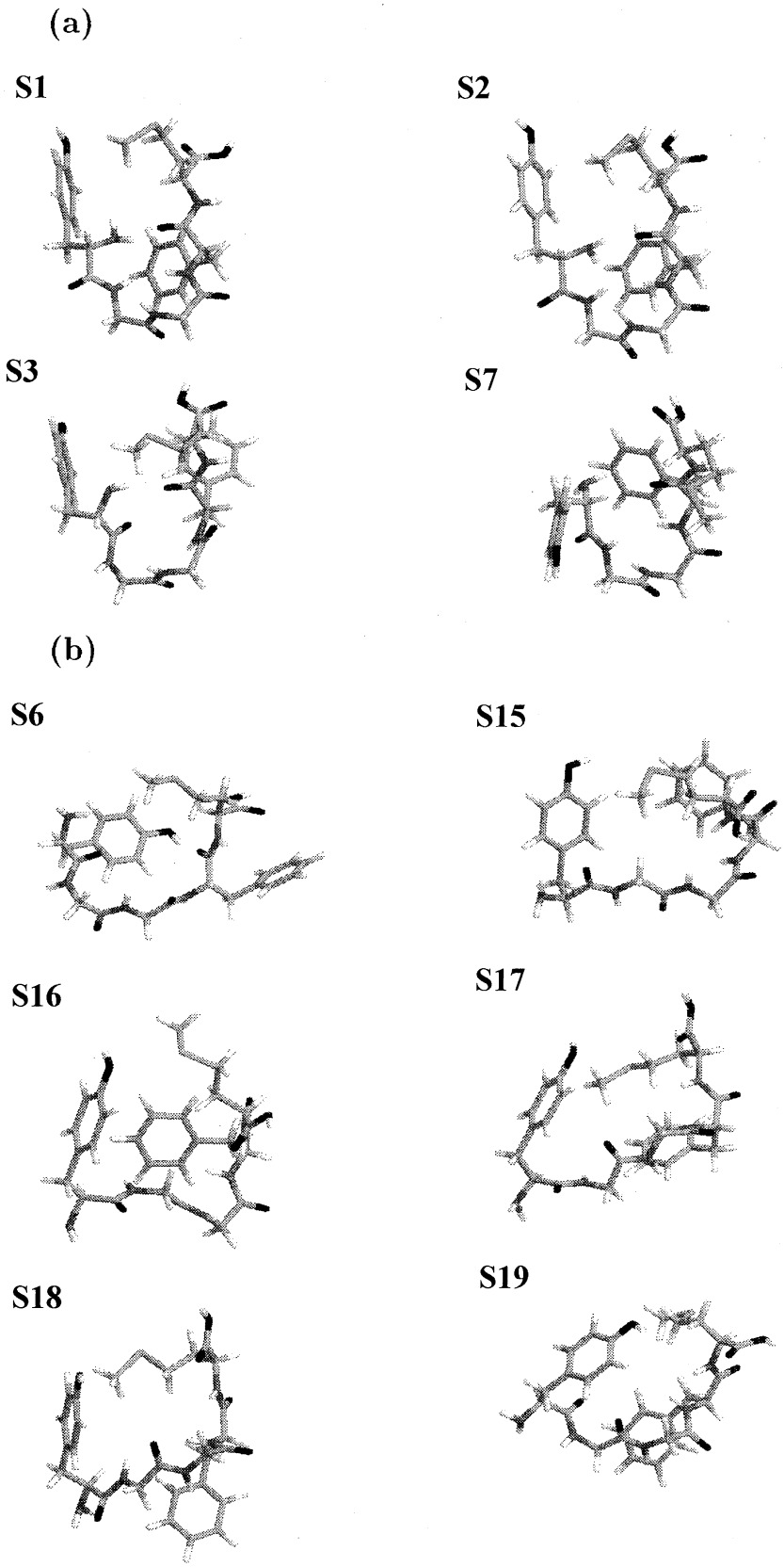

Fig. 5. Two kinds of conformations with low cavity-formation free energy: Conformations S1, S2, S3, and S7 (a), and S6 and from S15 to S19 (b). Structures in (a) have a hydrogen bond between the amide nitrogen of Tyr-1 and the carbonyl oxygen of Phe-4 backbone. Structures in (b) have circular shapes in which the main chain is extended and the N-terminal side-chain (Tyr-1) is very close to the C-terminal one (Met-5). The figures were created with Ras Mol.[26]

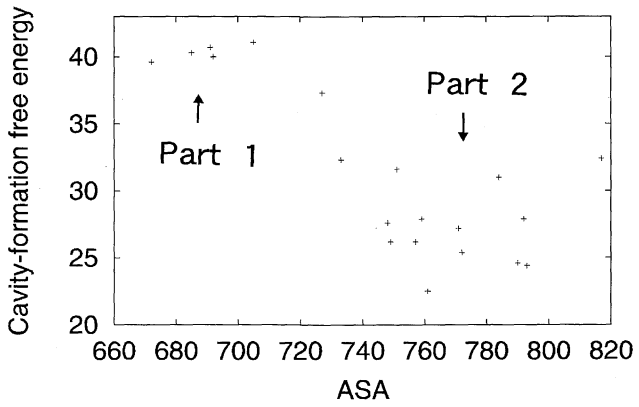

Fig. 6. Cavity-formation free energy (kcal mol^{-1}) of conformations as a function of solvent-accessible surface area (Å^2). The conformations are the lowest-energy conformations obtained in each of the 20 Monte Carlo simulated annealing runs in the solvent. It is found that there are two parts. One part (Part 1) corresponds to the structures that have high cavity-formation free energies and small accessible surface areas. These conformations are similar to those of group B in gas phase, which have two intrachain hydrogen bonds. The second part (Part 2) corresponds to the structures that have low cavity-formation free energies and large accessible surface areas. These structures have either circular shapes in which the main chain is extended but the N-terminal side chain (Tyr-1) is close to the C-terminal one (Met-5) or have a hydrogen bond between the amide nitrogen of Tyr-1 and the carbonyl oxygen of Phe-4 (one of the hydrogen bonds of group B is broken).

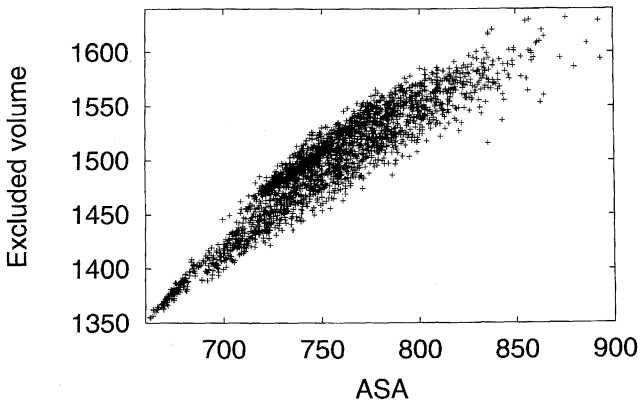

Fig. 7. The solvent-excluded volume (Å^3) of conformations obtained by three SA runs as a function of their accessible surface area (Å^2). One of the simulation runs, which we refer to as Run 1, was made so that it reproduces the one that gave the lowest-energy conformation in Part 1 of Fig. 6. Another run (Run 2) reproduces the lowest-energy conformation in Part 2 of Fig. 6. The third run (Run 3) was newly made. One conformation at each temperature with the increment of 1 degree (T = 150, 151, 152, ⋯, and 1000 K) was chosen for the analysis (total of 851 conformations for each run).

mations (E_{TOT} < 40 kcal mol^{-1}) in Run 2 has no correlation with the accessible surface area. These results show that cavity-formation free energy is not necessarily proportional to accessible surface area for a small peptide, such as Met-enkephalin, and depends on the microscopic structures of the peptide. This conclusion is in accord with the results of simulations of Met-enkephalin with RISM theory.[27]

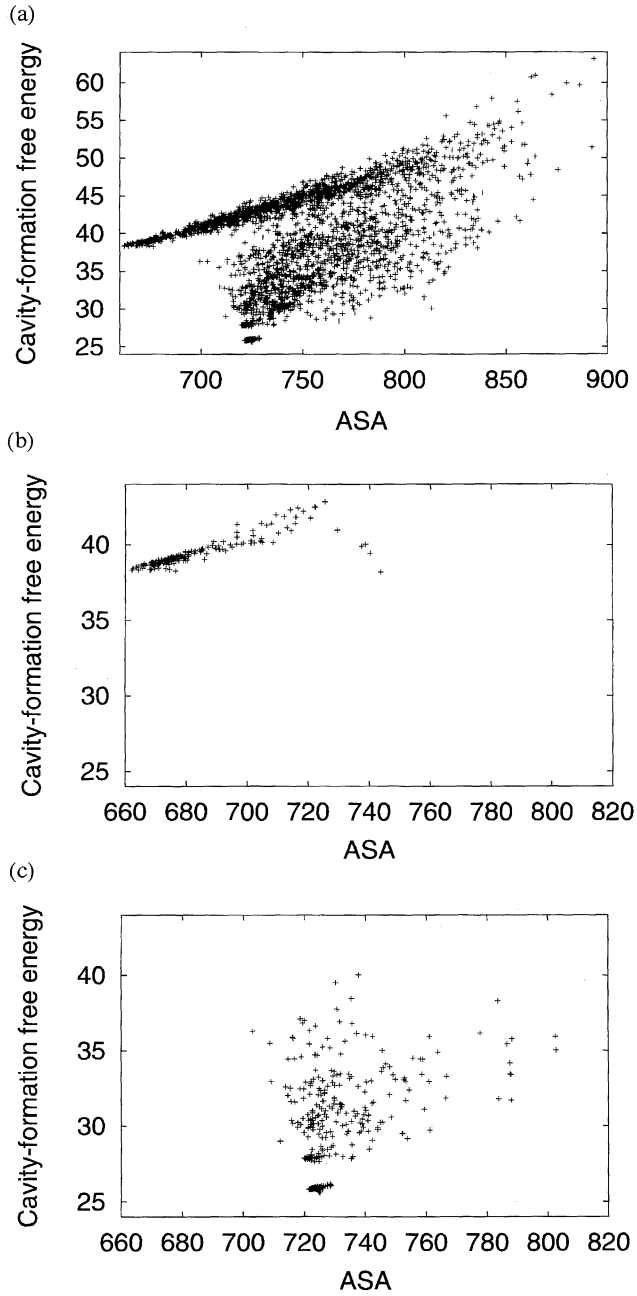

Fig. 8. Cavity-formation free energies of the conformations as a function of accessible surface area. The data from all 851×3 conformations are shown (a) (see the caption of Fig. 7). The data for (b) and (c) are from the conformations which have E_{TOT} < 40 kcal mol^{-1} in Run 1 and Run 2, respectively.

Conclusions

In this article, we have presented the results of Monte Carlo simulated annealing simulations of a penta peptide, Met-enkephalin, in the gas phase and in aqueous solution. We estimated a rigorous cavity-formation term in the sol-

vation free energy by the extended scaled particle theory. This was the first attempt to combine Monte Carlo simulated annealing and the extended scaled particle theory. We classified the conformations into groups of similar structures by calculating the root-mean-square distances between the atoms in backbone. It is found that the obtained conformations in the gas phase and in the solvent are both classified into three groups. It was also found that there is only one dominant low-energy structure in the solvent, while there are two dominant ones in the gas phase. The backbone of lowest-energy structure in the solvent has a shape similar to that of the second lowest-energy structure in the gas phase; the global-minimum-energy conformation in the gas phase was not found in the simulations in the solvent. It seems that the solvent effects decrease the number of low-energy local minima. Moreover, we studied in detail the relations between the solvent-accessible surface area and the cavity-formation free energy. It was shown that the cavity-formation free energy of the obtained conformations is not necessarily proportional to the accessible surface area for a small peptide such as Met-enkephalin. This implies that the cavity-formation free energy of a small peptide depends on its microscopic structure. The results should be taken as a warning when one uses emprical methods for calculating the solvation free energy based on the accessible surface area.

Finally, we remark that the lowest-energy conformation of Met-enkephalin obtained by simulations with rigorous solvation theory (RISM) is fully extended,[10] in agreement with the results of NMR experiments.[28] However, the lowest-energy conformation obtained by the present simulations using the extended scaled particle theory is rather round, although some of the low-energy conformations have extended backbone structures. Hence, we find that the neglected contributions (especially, the electrostatic interactions between solute and solvent molecules) are also important when we try to compare the simulation results with experiments.

The simulations were performed on computers at the Computer Center of the Institute for Molecular Science. This work was supported, in part, by grants from the Research Fellowship of the Japan Society for the Promotion of Science for Young Scientists (awarded to A. M.), from the Research for the Future Program (JSPS-RFTF98P01101) of the Japan Society for the Promotion of Science, and from the Ministry of Education, Science, Sports and Culture.

References

1 S. Kirkpatrick, C. D. Gelatt, Jr., and M. P. Vecchi, *Science*, **220**, 671 (1983).

2 B. A. Berg and T. Neuhaus, *Phys. Lett.*, **B267**, 249 (1991).

3 a) A. P. Lyubartsev, A. A. Martinovski, S. V. Shevkunov, and P. N. Vorontsov-Velyaminov, *J. Chem. Phys.*, **96**, 1776 (1992). b) E. Marinari and G. Parisi, *Euro-Phys. Lett.*, **19**, 451 (1992).

4 B. Hesselbo and R. B. Stinchcombe, *Phys. Rev. Lett.*, **74**, 2151 (1995).

5 U. H. E. Hansmann and Y. Okamoto, *Phys. Rev. E*, **56**, 2228 (1997).

6 D. Chandler and H. C. Andersen, *J. Chem. Phys.*, **57**, 1930 (1972).

7 F. Hirata and P. J. Rossky, *Chem. Phys. Lett.*, **83**, 329 (1981).

8 M. Kinoshita, Y. Okamoto, and F. Hirata, *J. Comput. Chem.*, **18**, 1320 (1997).

9 M. Kinoshita, Y. Okamoto, and F. Hirata, *J. Chem. Phys.*, **107**, 1586 (1997).

10 M. Kinoshita, Y. Okamoto, and F. Hirata, *J. Am. Chem. Soc.*, **120**, 1855 (1998).

11 H. Reiss, H. L. Fish, and J. L. Lebowitz, *J. Chem. Phys.*, **31**, 369 (1959).

12 R. A. Pierotti, *Chem. Rev.*, **76**, 717 (1965).

13 M. Irisa, T. Takahashi, F. Hirata, and T. Yanagida, *J. Mol. Liq.*, **65**, 381 (1995).

14 M. Irisa, T. Takahashi, K. Nagayama, and F. Hirata, *Mol. Phys.*, **85**, 1227 (1995).

15 a) F. A. Momany, R. F. McGuire, A. W. Burgess, and H. A. Scheraga, *J. Phys. Chem.*, **79**, 2361 (1975). b) G. Némethy, M. S. Pottle, and H. A. Scheraga, *J. Phys. Chem.*, **87**, 1883 (1983). c) M. J. Sippl, G. Némethy, and H. A. Scheraga, *J. Phys. Chem.*, **88**, 6231 (1984).

16 H. Kawai, Y. Okamoto, M. Fukugita, T. Nakazawa, and T. Kikuchi, *Chem. Lett.*, **1991**, 213.

17 Y. Okamoto, M. Fukugita, T. Nakazawa, and H. Kawai, *Protein Eng.*, **4**, 639 (1991).

18 M. Irisa, *Comput. Phys. Commun.*, **98**, 317 (1996).

19 a) B. Honig and A. Nicholls, *Science*, **268**, 1144 (1995). b) H. Nakamura, *Q. Rev. Biophys.*, **29**, 1 (1996).

20 T. Takahashi, H. Nakamura, and A. Wada, *Biopolymers*, **32**, 897 (1992).

21 J. P. M. Postma, H. J. C. Berendsen, and J. R. Haak, *Chem. Soc.*, **17**, 55 (1982).

22 K. Soda, *J. Phys. Soc. Jpn.*, **62**, 1782 (1993).

23 N. Metropolis, A. W. Rosenbluth, M. N. Rosenbluth, A. H. Teller, and E. Teller, *J. Chem. Phys.*, **24**, 1437 (1985).

24 Y. Okamoto, T. Kikuchi, and H. Kawai, *Chem. Lett.*, **1992**, 1275.

25 Z. Li and H. A. Scheraga, *Proc. Natl. Acad. Sci. U.S.A.*, **84**, 6611 (1987).

26 R. A. Sayle and E. J. Milner-White, *TIBS*, **20**, 374 (1995).

27 M. Kinoshita, Y. Okamoto, and F. Hirata, unpublished.

28 W. H. Graham, E. S. Carter, II, and P. R. Hickes, *Biopolymers*, **32**, 1755 (1992).